Extreme-ultraviolet polarization and filtering with gold transmission gratings

Earl E. Scime, Erik H. Anderson, David J. McComas, and Mark L. Schattenburg

The polarization and transmission characteristics of freestanding gold transmission gratings, with 200-nm periods, for extreme-ultraviolet (EUV) radiation ($l < 200$ nm) have been measured. We find that EUV transmission through the gratings is dominated by the waveguide characteristics of the gratings and that polarization efficiencies of 90% for wavelengths of 121.6 nm are achievable. Both the EUV polarization and transmission properties are in good agreement with a complete vector, numerical solution of Maxwell's equations. The fraction of open area to total area of the grating has been measured using a 10-keV proton beam and was found to be in good agreement with the microscopic slit and wire dimensions that were obtained by scanning electron microscopy. The use of these gratings for particle measurements in the presence of intense EUV radiation is briefly discussed.

Key words: Ultraviolet polarization, transmission gratings.

1. Introduction

Although the primary use of freestanding, submicrometer period, gold transmission gratings has been x-ray diffraction,[1–3] a number of other novel applications have been developed or proposed: grating-based extreme-ultraviolet monochromators,[4] extreme-ultraviolet polarizers,[5,6] and atom wave interferometers.[7,8] Our interest in these gratings arose from a need for a filter that would reject extreme-ultraviolet (EUV) light, in particular the 121.6-nm line of hydrogen, while permitting the passage of energetic neutral atoms (from 10 eV to 10 keV). The relative rejection (EUV to neutrals) required is 10^{10}. This level of EUV rejection is needed for a new class of spaceborne neutral atom imaging experiments that must detect neutral atoms in the presence of the intense 121.6-nm line reflected from the Earth's geocorona.[9] An operational schematic of our envisioned detector is shown in Fig. 1. It was suggested by Gruntman[5] that freestanding, submicrometer period gratings would make efficient EUV polarizers and would thus satisfy the EUV rejection requirement: neutral atoms pass through the remaining open area of two gratings that are oriented 90° to each other, and the EUV light is eliminated by the polarizing properties of the gratings.

We have measured the atomic and EUV transmission properties of freestanding, gold transmission gratings with 200-nm periods and have determined the polarization efficiency of a pair of these gratings for 121.1-nm light. The polarization efficiency of these gratings is not sufficient to achieve the necessary level of EUV rejection, but by utilizing the waveguide nature of the EUV transmission identified in this study, an EUV rejection of 10^{10} is possible.

2. Grating Description

Our gratings were constructed at the Massachusetts Institute of Technology's NanoStructures Laboratory using techniques developed for the Advanced X-ray Astrophysics Facility (AXAF) satellite.[10] The grating period is established upon a photoresist surface by an interference pattern (holographic lithography) that arises from the mixing of two beams of an argon-ion laser (351.1 nm). The resulting mask is processed further, permitting the deposition of gold between the bars of the mask. The remaining photoresist is then etched away, leaving a 200-nm period grating resting upon a layer of plating base material. Because the grating is too weak to support itself, two support gratings, fabricated by ultraviolet lithography, are superimposed atop the 200-nm period grating.

E. E. Scime and D. J. McComas are with the Los Alamos National Laboratory, Los Alamos, New Mexico 87545. E. H. Anderson is with the Lawrence Berkeley Laboratory, Berkeley, California 97420. M. L. Schattenburg is with the Center for Space Research, Massachusetts Institute of Technology, Cambridge, Massachusetts 02139.

Received 3 January 1994; revised manuscript received 5 July 1994.

0003-6935/95/040648-07$06.00/0.

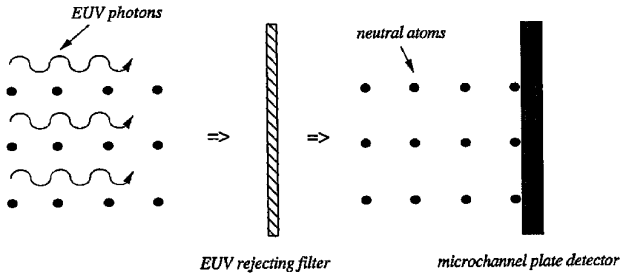

Fig. 1. Operational schematic of a neutral atom detector based on a filter that rejects EUV light while letting atoms pass through.

The support gratings have nominal periods of 4 and 150 μm, with the 4-μm period grating deposited orthogonally atop the 200-nm grating and the 150-μm period grating deposited orthogonally atop the 4-μm grating. The plating base is then etched away, leaving a freestanding, gold transmission grating. Figure 2(a) depicts a typical grating structure. The support structure typically has a transparency between 30% and 40% and currently available gratings have dimensions of 5 mm × 10 mm. Figures 2(b) and 2(c) are scanning electron microscope (SEM) photographs of a 200-nm period transmission grating consisting of 123.1-nm-wide bars with 76.9-nm-wide slits. The support structure is 37% transparent.

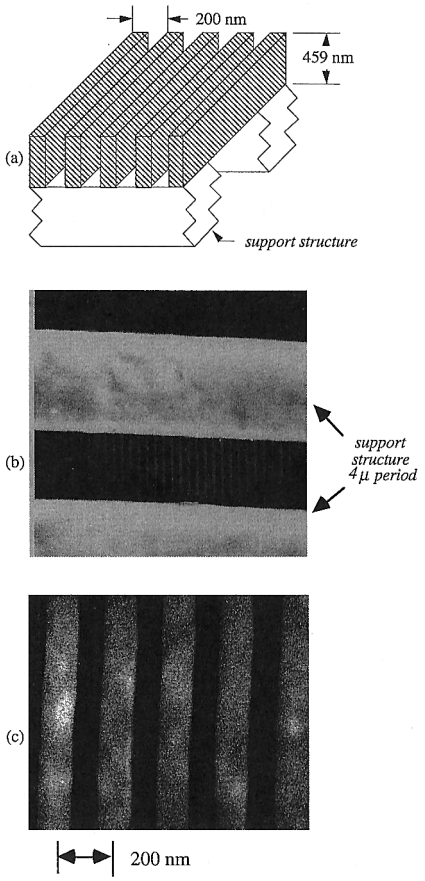

Fig. 2. (a) Schematic of the freestanding gold grating structure. (b) Grating viewed through a 4-μm period support structure with a SEM. (c) Enlarged view of a 200-nm period grating.

The transmission grating bars are 459 nm deep. Based on these measurements, the expected transmission of neutral atoms at normal incidence is 14%.

3. Particle Transmission Measurements

To determine the magnitude and uniformity of a grating's particle transmission, we illuminated the grating with a spatially uniform 10-keV proton beam. The proton flux that passes through the grating was measured with a microchannel plate (MCP) imaging system that consists of three stacked MCP's and a position-sensitive resistive anode placed behind the grating (Fig. 3).

Our initial particle transmission measurements were disappointing. The measured particle transmissions of gratings with expected transmissions of nearly 8% were less than 2% and highly nonuniform across the grating. An example of the spatial distribution of transmitted protons from a uniform illumination beam through a poorly transmitting grating is shown in Fig. 4. Because energetic photons can easily pass through thin blockages between the grating bars, these nonuniformities were not seen in x-ray studies that use these gratings.[10] Modifications in the manufacturing process based on our early results have significantly improved the grating particle transmission, both in magnitude and uniformity (Fig. 5). For the grating shown in Fig. 2, the measured particle transmission (shown in Fig. 6) was nearly 12%. The slight discrepancy between the measured and expected transmission, 12% versus 14%, is likely due to bulging of the sides of the bars into the slits, constricting them somewhat. Such bulging would not be visible in the SEM photographs because the secondary electrons produced at the grating surface and used for imaging by the SEM cannot escape from the deep slits. The small circular occlusion visible in Fig. 5 is either a piece of dust or a region of plating base that was not completely etched away during the manufacturing process. The angular acceptance of this grating, $\theta = \tan^{-1}(76.9/459) = 10°$, was confirmed by rotating the grating in the particle beam.

We have also measured the net particle transmission through two perpendicularly oriented gratings with individual particle transmissions of 8.6% and 12%. The net 10-keV proton transmission was 1%, exactly what would be expected from combining the individual transmissions.

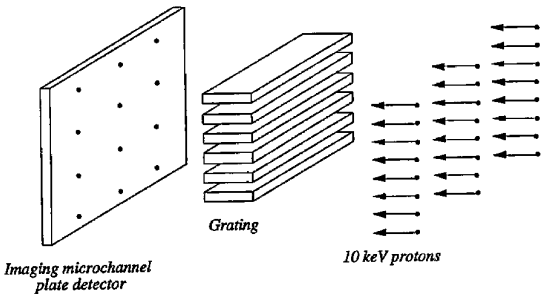

Fig. 3. Schematic of the proton illumination apparatus.

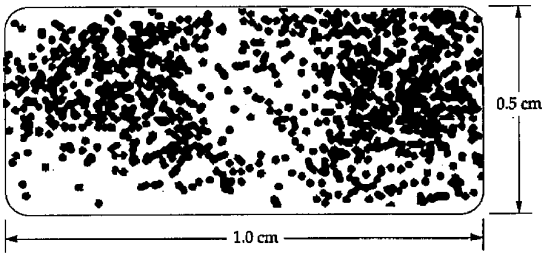

Fig. 4. 10-keV proton-illuminated image of the transmission grating showing, before the improvements in the manufacturing process, extremely poor and nonuniform transmission. Image has been artificially smoothed to enhance contrast and compensate for poor signal-to-noise levels.

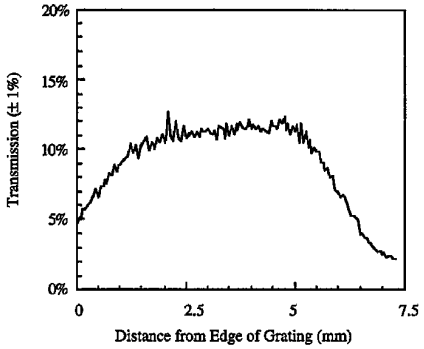

Fig. 6. Proton transmission for a narrow, shorter dimension cut through the grating image of Fig. 5.

4. Extreme-Ultraviolet Transmission and Polarization Measurements

The transmission of EUV and soft x-ray radiation through these gratings is considerably more complicated than for particles. The boundary conditions on the magnetic and electric fields inside the grating structure, as well as the effects of the finite resistivity of the gold grating on energy transport, determine the fraction of incident radiation that is transmitted through the grating. In wire grid polarizers that are used for microwave and infrared radiation,[11–13] polarization is achieved by the absorption and subsequent reemission of the component of the incident radiation for which the electric field is parallel to the wires; the parallel electric fields induce currents in the wires, whereas the component with its electric field perpendicular to the wires drives no current. The amplitudes of the reflected and transmitted waves have been calculated analytically for ideal, zero resistivity wires,[14] and attempts have been made to include resistive effects in similar calculations.[15] Both experiment and theory have demonstrated that the polarization efficiency decreases sharply as the radiation wavelength approaches the grating period.[16] Although there is every reason to believe that similar gratings with 10–20-nm periods would effectively polarize 121.6-nm radiation, construction of such gratings is beyond the capability of current technology. Our gratings have periods approximately twice as large as the primary radiation wavelength in which we are interested, 121.6 nm.

The situation of comparable period and radiation sizes has been examined analytically and computationally by a number of researchers.[17] We have used a computational model that was developed to simulate the diffraction of x rays through freestanding, gold transmission gratings,[18] in conjunction with our laboratory measurements, to understand the transmission of EUV radiation through such gratings. The code is based on a Floquet modal technique[19] and uses two complementary techniques to determine the coupled-mode (Floquet mode) eigenvalues for a square-wave structure. The code assumes that the grating is a perfect square-wave structure and has no variations along its depth. One can obtain a first estimate of the eigenvalues by solving for the eigenvalues of a matrix that results from a set of truncated Fourier-mode equations based on Maxwell's equations and the relevant boundary conditions. These eigenvalues are then used as a starting point for a Newton's method solution to a transcendental equation whose roots are the eigenvalues. The transcendental equation is based on the same equations and boundary conditions as the matrix approach, but the periodicity of the fields inside the grating is built into the equation. By using both methods in conjunction, the relatively slow and accurate Newton method benefits from an excellent set of starting points, and the errors introduced by truncating the Fourier series in the matrix method do not affect the final result.

The simulation was used to calculate the transmitted intensity of waves incident with electric fields parallel, transverse electric (TE), or perpendicular, transverse magnetic (TM), to the grating bars. The TE and TM transmissions through a 200-nm period grating (66.6-nm slits and 133.3-nm bars) as functions of grating thickness are shown in Fig. 7. The logarithmic decrease of transmitted power as a function of grating thickness is a well-known property of lossy waveguides that operate above cutoff or perfectly conducting waveguides that operate below cutoff,[20] thus the simulation predicts the grating functions as a parallel plate waveguide and not as an ideal polarizer; an ideal polarizer transmits exactly half of the incident unpolarized light. The waveguide nature of the grating demonstrated by the simulation is not surprising, as the aspect ratio (slit depth to slit width) of the grating is 5 or greater and the slits are many wavelengths deep. Waveguidelike propaga-

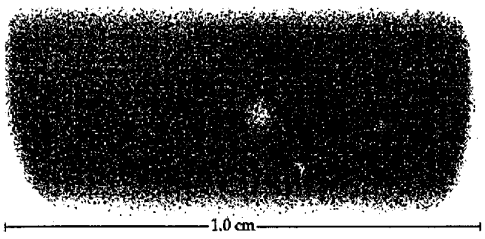

Fig. 5. 10-keV proton-illuminated image of the transmission grating, after the improvements in the manufacturing process, showing a small occlusion with uniform transmission elsewhere.

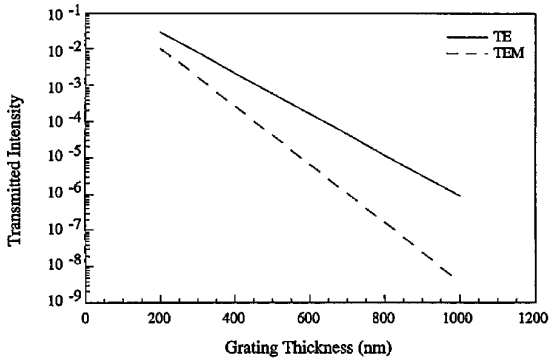

Fig. 7. TE and TEM transmission through a 200-nm period gold grating (66.6-nm slits and 133.3-nm bars) as a function of grating thickness at a wavelength of 121.6 nm.

tion of x rays in similar gratings has been demonstrated experimentally.[21]

As a check of the simulation, we compared the numerical results to analytical waveguide calculations. Simple equations for the transmitted powers of TE and TM modes that propagate in a parallel plate waveguide with resistive walls in the regime above cutoff are available.[22,23] It should be noted, however, that the TEM or $n = 0$ TM mode is also an allowed mode of propagation in a parallel plate waveguide. In fact, for plane, transverse waves in free space, $\mathbf{k} \times \mathbf{E} = \mathbf{k} \times \mathbf{B} = 0$, the perpendicularly polarized waves have no electric field component along $\mathbf{k}$, the propagation vector, and are best described as a TEM mode wave after they enter the waveguide. The TEM mode is the only purely transverse wave within the waveguide, as opposed to the TM waves that include an electric field component along $\mathbf{k}$. To satisfy the boundary conditions on the electric field, the incident waves polarized with their electric field parallel to the grating bars must propagate as TE mode waves in the parallel plate waveguide. For direct comparison of the numerical simulation with the analytical theory, we chose wavelengths and slit dimensions that were above cutoff for only the first TE mode (the TEM mode has no cutoff condition). In this regime, the attenuation coefficients, α, for the transmitted power, $W \propto \beta \exp(-2\alpha z)$, are given by[23]

$$\alpha_{\mathrm{TEM}} = R/b\xi, \tag{1}$$

$$\alpha_{\mathrm{TE}} = (2R/b\xi)\frac{(\lambda/2b)^2}{[1-(\lambda/2b)^2]^{1/2}}, \tag{2}$$

where β is the TEM or TE nondissipative waveguide transmission coefficient, b is the width of the slit, R is the grating material's characteristic resistance in ohms, λ is the incident wavelength, R/ξ is proportional to the frequency-dependent skin depth in the grating material and z is the grating thickness. The nondissipative waveguide amplitudes (β) are provided to indicate the relative transmissions at large periods. For a fixed wavelength of 121.6 nm, a grating thickness of 450 nm, a grating period of 200 nm, and a fixed slit width to period (P) ratio of 33:100 ($P = 3b$), the EUV transmission as a function of grating period obtained from the numerical simulation is shown in Fig. 8 (curves). Tabulated values of the optical properties of gold were used in the numerical simulation.[24] The transmissions based on Eqs. (1) and (2) are also shown in Fig. 8 (diamonds) for the regime over which they are valid. Note that the TEM mode is attenuated more than the TE mode until the slit dimension is smaller than the wavelength and all possible TE modes are evanescent. Typical wire grid polarizers for microwaves or infrared radiation operate in the $P \ll \lambda$ regime, resulting in efficient polarizers. This is clearly not the case for the gratings examined here.

The total EUV transmission for two slightly different gratings was measured using a soft x-ray/EUV source constructed at Los Alamos to calibrate the ALEXIS x-ray telescope (ALEXIS stands for array of low-energy x-ray imaging sensors).[25] The source used a standard Penning discharge placed at the entrance slit of a grazing incidence, x-ray monochromator. The EUV transmission through both gratings for four different wavelengths is shown in Fig. 9. The low source flux of the ALEXIS facility, $\sim 10^3$ photons/s/cm^2, required long integration times to achieve reasonable signal-to-noise levels for measurements of transmissions of the order of 10^{-4}. As predicted by the simulation, neither grating functioned as a perfect polarizer at 121.6 nm or the other wavelengths; for a perfect polarizer with the open area of grating FS-177 and randomly polarized light the expected transmission is $0.5 \times (76.9/200) \times 0.37 = 0.07$. For comparison, the simulation-predicted transmissions are also shown in Fig. 9 (curves). The SEM measured grating and support structure dimensions were used in the simulation. The skin depth of radiation in the 50–200-nm wavelength range is approximately 13–26 nm for gold, thus surface imperfections in the gratings can be safely ignored in the simulation. To estimate the polarization of the source, which enters into the simulation results by the relative weighting of the TM and TE components, a single grating (identified

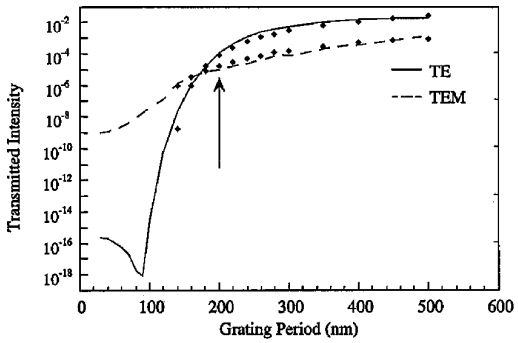

Fig. 8. Predicted TE and TEM transmissions through a 450-nm-thick gold grating from the simulation for a fixed wavelength of 121.6 nm as a function of period (curves) as well as the transmissions based on Eqs. (1) and (2) (diamonds). Bar widths of 133.3 nm and slit widths of 66.6 nm were used in both cases. The vertical arrow marks the period of gratings used in this study.

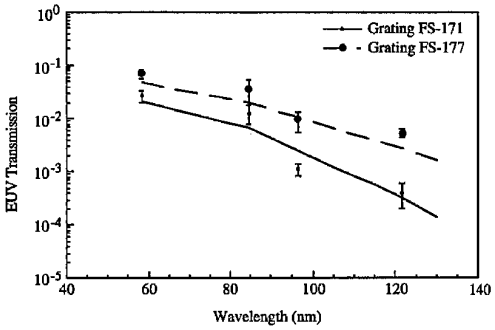

Fig. 9. Experimentally determined EUV transmission for two different gratings as a function of wavelength (circles) and the predicted transmissions from the simulation (solid curve).

as FS-171 in Fig. 9) was rotated in the 121.6-nm beam that exits the monochromator, and we assumed that the relative transmission of TM versus TE of approximately 1:11 at 121.6 nm predicted by the simulation was accurate. The simulation prediction has an error of at least ±20% because of the large variance in the available measurements of the optical properties of gold at these wavelengths. The estimated source polarization for each wavelength was then used to generate the theoretical transmission values used for grating FS-177 (Fig. 9). The agreement between theory and measurement for grating FS-177 supports the results of the estimated source polarization calculation. A more precise transmission measurement would require an EUV source with a well-known polarization, e.g., a synchrotron source, or an unpolarized source with a precisely measured polarizer.

The total transmission versus wavelength measurements using the ALEXIS source, while useful, do not yield any information about the polarizing properties of the gratings. To obtain polarization information, we measured the total transmission through two crossed gratings as a function of the angle subtended by their axes. Because the net EUV transmission of the two gratings was expected to be of the order of 10^{-7}–10^{-8}, we could not use the low-intensity ALEXIS facility (integration times of days would have been required). Instead we used a deuterium lamp continuum source ($120\ \text{nm} < \lambda < 170\ \text{nm}$). Since the detection efficiency of our MCP's is greatest for shorter EUV wavelengths,[26] we expected that the transmission measurements made by using the deuterium lamp would be dominated by the wavelengths closest to 120 nm. In fact, the deuterium lamp-based measurements were identical to the results that were obtained with the ALEXIS facility at 121.6 nm.

The intensity of the transmitted radiation through a single grating, I, is the sum of the transmitted intensities of the perpendicular and parallel components:

$$I = I_\perp + I_\parallel = T_\perp{}^2 + T_\parallel{}^2, \tag{3}$$

where $T_\perp$ and $T_\parallel$ are the transmitted amplitudes of each component of incident radiation. For the general case of a partially polarized source, this expression becomes

$$I = A^2 I_\perp + B^2 I_\parallel, \tag{4}$$

where $A^2 + B^2 = 1$. Malus law for the transmitted intensity through two polarizers whose axes of polarization are oriented at an angle θ with respect to each other can be generalized to include both transmitted components and the possibility of nonidentical polarizers:

$$I(\theta) = \cos^2\theta(A^2 T_{\parallel a}{}^2 T_{\parallel b}{}^2 + B^2 T_{\perp a}{}^2 T_{\perp b}{}^2) + \sin^2\theta(A^2 T_{\parallel a}{}^2 T_{\perp b}{}^2 + B^2 T_{\perp a}{}^2 T_{\parallel b}{}^2), \tag{5}$$

where a and b identify each of the two gratings. This expression can be written in terms of the transmitted intensity at $\theta = 0°$ and $\theta = 90°$:

$$I(\theta) = I(0°)\cos^2\theta + I(90°)\sin^2\theta, \tag{6}$$

and for randomly polarized incident radiation, $A^2 = B^2 = 1/2$,

$$\frac{I(0°) - I(90°)}{I(0°) + I(90°)} = \chi_a \chi_b, \tag{7}$$

where χ is the polarization of each grating. So by measuring the transmitted intensity at 0° and 90° we can determine the effective polarization, $\sqrt{\chi_a \chi_b}$, of the grating pair.

The normalized transmitted intensity versus angle subtended by two gratings is shown in Fig. 10. The 90° measurement is equivalent to a total transmission of 2×10^{-6}. Also shown in Fig. 10 is Eq. (6). The gratings clearly function as partial polarizers in the manner predicted by Eq. (6). The simulation-predicted polarizations of each grating yield an effective polarization for the grating pair of 78%, compared with the measured value of 80.5%. The agreement between the simulation and measurements confirms that the component transmissions (TE and TM) predicted by the model are as reliable as the total transmission values.

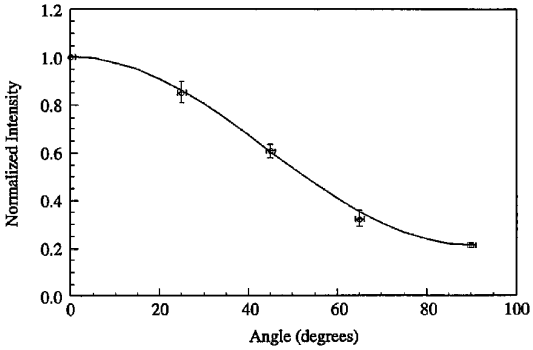

Fig. 10. EUV transmission (predominately $\lambda \approx 121.6$ nm) versus angle between two gratings: data (circles), modified Malus law, Eq. (6) (curve).

5. Discussion

Our measurements and modeling of these gold transmission gratings clearly indicate that, for EUV radiation, these gratings function as parallel plate waveguidelike structures. The polarization measurements yield polarizing efficiencies that are substantial for EUV wavelengths but are not sufficient to achieve our goal of an EUV rejection level of 10^{10} solely through polarization effects. The measured polarization efficiencies do, however, contradict the results of Ogawa *et al.*[3] who claimed that the polarizing properties of these gratings are insignificant based on their measurements of larger TE than TEM transmissions for wavelengths of 25.5, 30.4 and 34.0 nm. Our numerical and analytical results demonstrate (see Fig. 8) that the transmitted intensity of TE-polarized radiation should be greater than that of TEM for wavelengths shorter than the grating slit width.

Using two gratings with the characteristic waveguide attenuation of the best grating used in this study and including the detection efficiency of standard MCP's for 121.6-nm photons (1%) relative to energetic (keV) particles (80%),[27] the best relative rejection achievable is 10^8. A third grating could be used to achieve a 10^{10} rejection, but a net neutral atom transmission of 0.1% would result in unacceptable signal-to-noise levels for a neutral atom imager.[9] There are at least three simple ways to increase the EUV rejection by 2 orders of magnitude and maintain or even increase the net neutral atom transmission. First, the two gratings could be made slightly thicker, an increase from 450 to 600 nm would be more than sufficient (see Fig. 7) to increase the EUV rejection level for a two-grating-based neutral atom imager to 10^{10}. Second, a single very thick grating ($\sim$1300 nm) would have an EUV transmission of $\sim 10^{-9}$ (see Fig. 7) and a neutral atom transmission of 10%, yielding an imager with a relative EUV rejection of 10^{10}. Or third, since it is the lossy waveguide properties of the gratings that dominate the transmission characteristics for our application, silver could be used instead of less resistive gold. Silver-based simulations predict an improvement of an order of magnitude in the relative transmission of gratings identical to those used in this study. Construction of thicker gratings is in progress, and we believe that an instrument that consists of two crossed gratings and an imaging MCP detector will achieve an EUV to neutral atomic flux rejection level of 10^{10} in the near future.

The Los Alamos National Laboratory portion of this work was performed under the auspices of the U.S. Department of Energy. The Lawrence Berkeley Laboratory portion of this work was supported by the Director, Office of Energy Research, Office of Basic Energy Science, U.S. Department of Energy under contract DE-AC03-76SF00098. The authors thank Frank Ameduri, Bob Baldonado, and Danny Everett for technical support, Monica Coakley for helpful discussions, and the ALEXIS team for the use of the ALEXIS calibration facility. One of the authors (E. E. Scime) was also supported by the Department of Energy Distinguished Postdoctoral Research Program administered by the Oak Ridge Institute for Science and Education.

References

1. M. L. Schattenburg, E. H. Anderson, and H. I. Smith, "X-ray/VUV transmission gratings for astrophysical and laboratory applications," Phys. Scr. **41,** 13–20 (1990).
2. H. Lochbihler and P. Predehl, "Characterization of x-ray transmission gratings," Appl. Opt. **31,** 964–971 (1992).
3. H. W. Ogawa, D. R. McMullin, D. L. Judge, and R. Korde, "Normal incidence spectrophotometer with high-density transmission grating technology and high-efficiency silicon photodiodes for absolute solar extreme-ultraviolet irradiance measurements," Opt. Eng. **32,** 3121–3125 (1993).
4. P. J. Caldwell, E. T. Arakawa, and T. A. Callcott, "Extreme ultraviolet transmission grating monochromator," Appl. Opt. **20,** 3047–3050 (1981).
5. M. A. Gruntman, Submicron structures: promising filters in EUV—a review," in *EUV, X-Ray, and Gamma-Ray Instrumentation for Astronomy,* R. E. Rothschild and O. H. Siegmund, eds., Proc. Soc. Photo-Opt. Instrum. Eng. **1549,** 385–394 (1991).
6. G. J. Sonek, D. K. Wagner, and J. M. Ballantyne, "Ultraviolet grating polarizers," J. Vac. Sci. Technol. **19,** 921–923 (1981).
7. D. W. Keith, M. L. Schattenburg, H. I. Smith, and D. E. Pritchard, "Diffraction of atoms by a transmission grating," Phys. Rev. Lett. **61,** 1580–1583 (1988).
8. D. W. Keith, C. R. Ekstrom, Q. A. Turchette, and D. E. Pritchard, "An interferometer for atoms," Phys. Rev. Lett. **66,** 2693–2696 (1991).
9. D. J. McComas, B. L. Barraclough, R. C. Elphic, H. O. Funsten III, and M. F. Thomsen, "Magnetospheric imaging with low energy neutral atoms," Proc. Natl. Acad. Sci. USA **88,** 9598–9602 (1991).
10. M. L. Schattenburg, C. R. Canizares, D. Dewey, K. A. Flanagan, M. Hamnett, A. M. Levine, K. S. K. Lum, R. Manikkalingam, T. H. Markert, and H. I. Smith, "Transmission grating spectroscopy and the Advanced X-Ray Astrophysics Facility (AXAF)," Opt. Eng. **30,** 1590–1600 (1991).
11. J. P. Auton, "Infrared transmission polarizers by photolithography," Appl. Opt. **6,** 1023–1027 (1967).
12. Y. S. Hwang and H. K. Park, "Polarization characteristics of wire mesh at 119 μm," Appl. Opt. **28,** 4999–5001 (1989).
13. J. P. Casey and E. A. Lewis, "Interferometer action of a parallel pair of wire gratings," J. Opt. Soc. Am. **42,** 971–977 (1952).
14. W. V. Ignatowsky, "Zur Theorie der Gitter," Ann. Phys. **44,** 369–437 (1914).
15. E. A. Lewis and J. P. Casey, Jr. "Electromagnetic reflection and transmission by gratings of resistive wires," J. Appl. Phys. **23,** 605–608 (1952).
16. G. R. Bird and M. Parrish, Jr., "The wire grid as a near-infrared polarizer," J. Opt. Soc. Am. **50,** 886–891 (1960).
17. R. Petit, *Electromagnetic Theory of Gratings* (Springer-Verlag, Berlin, 1980).
18. E. H. Anderson, "Fabrication and electromagnetic applications of periodic nanostructures," Ph.D. dissertation (Massachusetts Institute of Technology, Cambridge, Mass., 1988).
19. R. Magnusson and T. K. Gaylord, "Equivalence of multiwave coupled-wave theory and modal theory for periodic media diffraction," J. Opt. Soc. Am. **68,** 1777–1779 (1978).
20. J. D. Jackson, *Classical Electrodynamics* (Wiley, New York, 1975), p. 348.

21. N. M. Ceglio, A. M. Hawryluk, and D. G. Stearns, "Demonstration of guided-wave phenomena at extreme-ultraviolet and soft-x-ray wavelengths," Opt. Lett. **13,** 267–269 (1988).
22. R. I. Sarbacher and W. A. Edson, *Hyper and Ultrahigh Frequency Engineering* (Wiley, New York, 1944), p. 174.
23. N. Marcuvitz, *Waveguide Handbook* (McGraw-Hill, New York, 1951), pp. 62–65.
24. D. E. Gray, ed., *American Institue of Physics Handbook* (McGraw-Hill, New York, 1972), pp. 6–118.
25. W. C. Preidohorsky, J. J. Bloch, B. C. Edwards, D. C. Roussel-Dupré, B. W. Smith, and O. H. W. Siegmund, "ALEXIS experiment and small satellite: initial on-orbit results," in *EUV, X-Ray and Gamma-Ray Instrumentation for Astronomy IV,* O. H. Siegmund, ed., Proc. Soc. Photo-Opt. Instrum. Eng. **2006,** 114–126 (1993).
26. F. Paresce, "Quantum efficiency of a channel electron multiplier in the far ultraviolet, Appl. Opt. **14,** 2823–2824 (1975).
27. T. Sakuri and T. Hashizume, "Determination of the detection efficiency of a channel plate electron multiplier," Rev. Sci. Instrum. **57,** 237–239 (1985).